



Dextran-based Hydrogel Layers for Biosensors

8

Andras Saftics, Barbara Türk, Attila Sulyok, Norbert Nagy, Emil Agócs, Benjámín Kalas, Péter Petrik, Miklós Fried, Nguyen Quoc Khánh, Aurél Prósz, Katalin Kamarás, Inna Szekacs, Robert Horvath, and Sándor Kurunczi

Abstract

Biofunctional coatings are key elements of biosensors regulating interactions between the sensing surface and analytes as well as matrix components of the sample. These coatings can improve sensing capabilities both by amplifying the target signal and attenuating interfering signals originating from surface fouling (non-specific binding). Considering the tested materials so far, hydrogel-based layers have been verified to be among the most effective layers in improving biochip performance. The polysaccharide dextran can be efficiently used to form hydrogel layers displaying extended three-dimensional structure on biosensor surfaces. Owing to their high water content and flexible structure, dextran coatings present advanced antifouling abilities, which can be exploited in classic bioanalytical measurements as well as in the development of cell-on-a-chip

A. Saftics · B. Türk · A. Prósz · I. Szekacs · R. Horvath (✉) · S. Kurunczi
Nanobiosensorics Laboratory, Centre for Energy Research, Hungarian Academy of Sciences, Budapest, Hungary

A. Sulyok
Thin Film Physics Department, Centre for Energy Research, Hungarian Academy of Sciences, Budapest, Hungary

N. Nagy · E. Agócs · B. Kalas · P. Petrik · M. Fried
Photonics Department, Centre for Energy Research, Hungarian Academy of Sciences, Budapest, Hungary

N. Q. Khánh
Microtechnology Department, Centre for Energy Research, Hungarian Academy of Sciences, Budapest, Hungary

K. Kamarás
Institute for Solid State Physics and Optics, Wigner Research Centre for Physics, Hungarian Academy of Sciences, Budapest, Hungary

type biosensors. However, in spite of the numerous applications, the deep characterization of dextran layers has been missing from the literature. This phenomenon can be attributed to the challenging analysis of few nanometer-thick layers with high water content. The lack of available data is more pronounced regarding the layer behaviors under aqueous conditions. In this chapter we present various surface analytical methods (including biosensor-type techniques) suitable for the complex characterization of hydrogel coatings whose thickness ranges from few to several ten nanometers. As a case study, we focus on the analysis of carboxymethyl dextran (CMD) layers developed for waveguide-based label-free optical biosensor applications. Examination methodologies both under dry and aqueous conditions as well as testing of antifouling abilities are also presented.

Keywords

Dextran · Hydrogel · Label-free biosensor · OWLS · QCM · Ellipsometry · Non-specific binding

8.1 Introduction

The role of biofunctional coatings is the modification of solid supports (substrates) by thin films (thickness is usually below 1 μm) of synthetic or naturally derived materials using various types of surface chemistries. Generally, the aim of modification is to maintain the desired and controlled interaction between the support and the biological system (Knoll 2013). In the field of biosensors, although biofunctional coatings are usually not defined as special sensor elements, they are of high importance in exploiting specific and detectable signals from biosensor response (Chandra 2016; Chandra et al. 2017). These coatings or so-called interface chemistries make the sensitization of the transducer surface by biorecognition elements possible. The role of biosensor coatings is more significant when the detection is based on a label-free method. Label-free biosensors measure signals generated only by the physical presence of analytes (targets). Due to this detection principle, all kinds of sample components present in the detectable field (mainly on the sensor surface) can produce signal which is therefore interfered by the non-targets as well. This type of interference is called biofouling or more specifically non-specific binding (NSB). As a result of the fact that protein molecules are main components of biological samples and they can adsorb to various surfaces, the NSB signal originates primarily from proteins. Additionally, as the adhesion of mammalian cells is mediated by surface-protein interactions, adsorbed proteins promote the biofouling of surfaces by cells and cell clusters. The essential aim of using well-designed biofunctional coatings on biosensor surfaces is the minimization of biofouling by a protein- and cell-repellent layer and furthermore the amplification of the target-related specific signal. It has been shown that the thermodynamically unfavorable

water exclusion in case of heavily hydrated coatings made of hydrogels significantly contributes to the protein-repellent abilities (Tanaka et al. 2013).

Hydrogels are hydrophilic polymers which are able to absorb large amount of water. Hydrogels have found applications in a number of fields including drug delivery systems (Sivakumaran et al. 2011; Secret et al. 2014; Liu et al. 2016), tissue engineering (Balakrishnan and Banerjee 2011; Zhang and Khademhosseini 2017; Liu et al. 2017; Xu et al. 2018) or biosensors (Mateescu et al. 2012; Lian et al. 2016; Peppas and Van Blarcom 2016; Tavakoli and Tang 2017). Hydrogel-based coatings are key elements of biosensors. The widespread application of hydrogels in biosensor design originates from surface plasmon resonance (SPR)-based biochip developments. The layers are designed to modify the physicochemical properties of the sensor transducer surface, which is originally not biocompatible, promotes the non-specific adsorption of proteins, and has reduced specific surface area (low immobilization capacity). The large number of conjugable sites provided by the 3D polymer network allows to accommodate huge amount of various biomolecules. Hydrogels provide a natural-like wet microenvironment for biomolecules enabling to maintain their stability. The structural similarity to the extracellular matrix (ECM), the porous framework, and – mainly in case of naturally derived polymers – the biomimetic characteristic all provide great benefits for cell survival, proliferation, and migration (Balakrishnan and Banerjee 2011; Liu et al. 2017).

The naturally derived polysaccharide dextran can be used to form high capacity hydrogel layers on biosensor chip surfaces improving measurement sensitivity. Also, conjugated with suitable anchor molecules, dextran can provide a mechanical support and ECM-mimicking microenvironment for living cells. Dextran is constructed of α -(1,6) linked anhydroglucose units in its linear chains. Its flexible branches (providing ca. 5% branching degree) are linked by α -(1,3) glycoside bonds. The dextran chemical structure can be seen in Fig. 8.1A. Using dextran layers on biosensor surfaces has been proven to be an efficient strategy to limit the NSB, increase the number of immobilized bioreceptors, and achieve higher signal-to-noise ratio, resulting in better sensitivity. The advanced antifouling ability of dextran mainly originates from its hydrophilic nature and flexible chains. The free motion of mobile chains plays a key role in generating high interfacial entropy and thus steric repulsion that has a determinate contribution (steric-entropic effect) against protein adsorption (Löfås and Johnsson 1990; McArthur et al. 2000; Massia et al. 2000).

Dextran layers present remarkable water absorption and swelling, resulting in even four times of increase in their thickness (Elender et al. 1996; Piehler et al. 1999). Originally, the term hydrogel is used for crosslinked polymers; however, without sticking to the pure definition, one can point that even layers made of uncrosslinked dextran present hydrogel properties or at least hydrogel-like behavior (Elam et al. 1984; Löfås and Johnsson 1990).

Owing to the biocompatibility, biomimetic characteristic, and ECM-like viscoelastic properties, hydrogels made of dextran derivatives are effectively used in tissue engineering as scaffolds and ECM model components (Ferreira et al. 2004; Lee et al. 2008; Cutiungco et al. 2014).

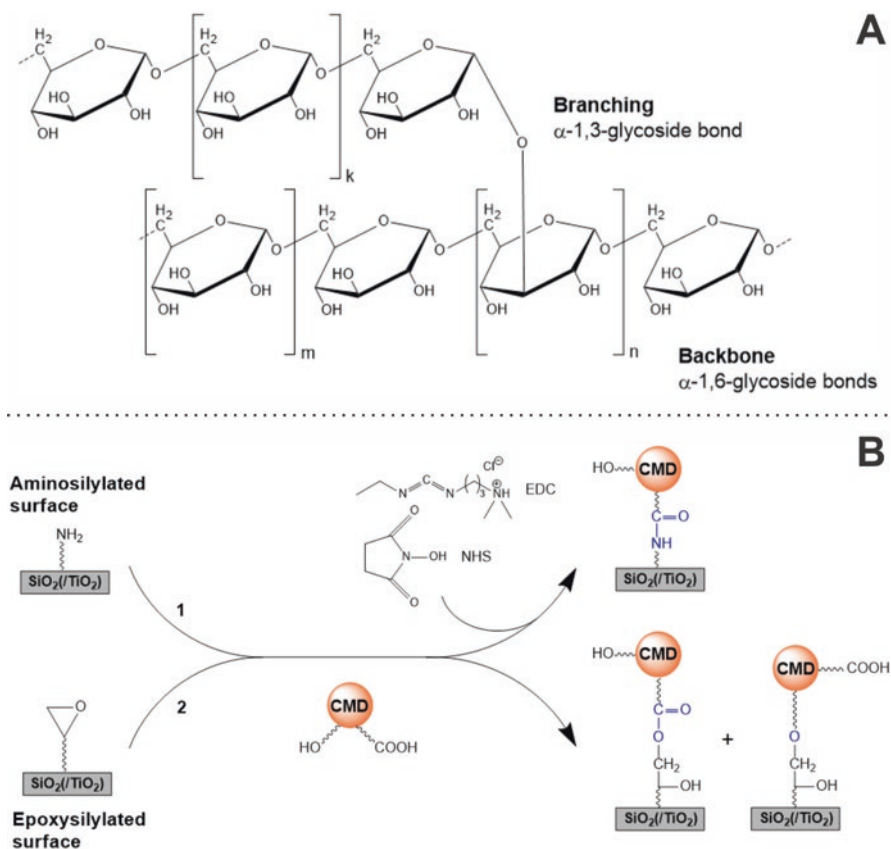


Fig. 8.1 (A) Chemical structure of dextran. The subscriptions m , n , and k indicate the number of anhydroglucose units in the backbone (m), branches (n), and branched chains (k). [Reprinted with permission from (Saftics 2018)]. (B) Reaction schemes of covalent grafting to amino- and epoxysilylated surfaces. While using aminosilane coating (1), EDC and NHS reagents are required, and the grafting chemistry results in amide bonds between the surface amino groups and CMD molecules. The grafting chemistry of using epoxide groups (2) can be performed without additional reagents, and it can form both ester and ether bonds between CMD and the surface. [Adapted with permission from (Saftics et al. 2016), copyright 2016 Elsevier]

Combining the achievements of biosensors and tissue engineering, label-free biosensors endowed with dextran-based hydrogel coatings are unique tools for revealing the surface-related events of cell clusters or even single cells, such as cell-cell or substrate-cell adhesion, spreading, migration, proliferation, and signaling. In spite of the number of advantageous properties and verified applications, dextran layers – mainly their structure – are poorly characterized, and descriptions about their fabrication methods are insufficient. The few available details about these coatings can be derived from the fact that the characterization of ultrathin, nanometers thick, and heavily hydrated polymer layers is still difficult and challenging, even with using the currently available modern surface analytical techniques.

To reveal the properties and dynamic behavior of such coatings, the deployment of various measurement techniques is in demand. Besides the classical bioanalytical applications, label-free biosensors and their unique surface sensitivity can be efficiently used to explore the structure and hydration of deposited polymer chains on sensing surfaces.

In this book chapter, we focus on the characterization of CMD hydrogel layers developed for various waveguide-based optical biosensor applications, such as for the analysis of controlled adhesion of living single cells and cell clusters. Due to the proposed future applications, the detailed analysis of the developed layers was highly demanded. We present our analytical methodologies applied for the characterization of layers both under dry and hydrated conditions. Regarding the different layer properties examined, our work covers the composition, topography, thickness, and wettability of the coatings. To reveal the hydration behavior and nanostructure in aqueous environment, both optical and mechanical biosensor techniques were employed. The analysis of the layers antifouling abilities is also presented.

8.2 Fabrication of Carboxymethyl Dextran Layers

Methods providing the surface grafting of stable dextran-based hydrogel layers with sufficient surface amount and thickness as well as with great antifouling ability and immobilization capacity are still under intensive research (Zhang and Horváth 2003). Generally, the fabrication of dextran layers is primarily empirically optimized, the published methods do not describe specific technical details, and the shared procedures are confusing in several cases.

Regarding the first biosensor applications, dextran layers were developed for SPR type sensors, therefore the original grafting methods apply thiol-based surface chemistries to attach dextran chains onto the gold surface of SPR chips (Löfås and Johnsson 1990; Löfås et al. 1993, 1995; Monchaux and Vermette 2007). Grafting methods to silica (glass) type surfaces are also available and can be used to functionalize waveguide-based optical transducers with dextran layers. These chemistries are mainly based on the silylation of the substrate resulting in a covalently bound silane film. This silane self-assembled monolayer (SAM) provides active functions for the covalent attachment of polysaccharide molecules. The most common silane reagents are epoxy- and aminosilanes (e.g., 3-glycidoxypropyltriethoxy silane (GOPS) and 3-aminopropyltriethoxysilane (APTES)). While CMD can directly react with epoxide groups both through its hydroxyl and carboxyl functions, the coupling of CMD via surface amino groups needs additional reagents, 1-ethyl-3-(3-dimethylaminopropyl)-carbodiimide hydrochloride (EDC) and N-hydroxysuccinimide (NHS) (Akkoyun and Bilitewski 2002). The EDC/NHS-based linking method is widely used, originally when protein molecules are intended to be coupled to other amine- or carboxyl-bearing surfaces or biomolecules. These grafting techniques are generally result in ultrathin layers whose thickness is typically in the range of 0.2–3.0 nm under dry conditions (Elender et al. 1996; Kuhner and Sackmann 1996). Thicker layers of polymers (thickness over 10–100 nm) can

be achieved by the spin-coating method that is based on the spreading of a polymer solution on flat surfaces while the substrate is rotated. However, there are only very few available methods on the fabrication of dextran-based coatings using spin-coating, and they avoid detailing the stability of the layers. Specifically, procedures based on the combination of spin-coating and crosslinking in dextran layer fabrication have not been published so far, only examples for simple spin-coating of dextran can be found (Piehler et al. 1999; Linder et al. 2005).

In this study, we present the characterization of two different types of CMD layers varying in their thickness and presence of chemical crosslinks. We developed ultrathin (hereafter CMD-ut layers) as well as thicker (10–100 nm) CMD layers, in the latter case using spin-coating technique with adding crosslinking agent to the coating solution (hereafter CMD-sc layers). For the fabrication of CMD-ut layers, aminosilane- (CMD-ut-Am layers) and epoxysilane-based (CMD-ut-Ep layer) coupling chemistries were both applied (see Fig. 8.1B). The layers were prepared on SiO₂-TiO₂ waveguide type substrates and Si model wafers. The deposition of CMD layers onto the silylated substrate was performed using batch and flow-cell methods. The fabrication of CMD-sc coatings involved the grafting of a CMD-ut layer onto an aminosilylated substrate and then the spin-coating of CMD solution that contained sodium trimetaphosphate (STMP) as a crosslinker. Regarding both the prepared CMD-ut and CMD-sc layers, the samples were intensively washed to gain their stable form. Detailed fabrication methods of these layers can be found in our previous publications (Saftics et al. 2016, 2017, 2018).

8.3 CMD Layer Characterization

8.3.1 Surface Analytical Techniques

Various surface analytical techniques were used to characterize the developed CMD layers, including attenuated total reflection Fourier-transform infrared spectroscopy (ATR-FTIR), x-ray photoelectron spectroscopy (XPS), atomic force microscopy (AFM), spectroscopic ellipsometry (SE), contact angle (CA) measurements, optical waveguide lightmode spectroscopy (OWLS), quartz crystal microbalance with impedance measurement (QCM-I), as well as phase contrast microscopy. A list of the used analytical techniques as well as specific layer parameters offered by the measurement methods are summarized in Table 8.1. In the following sections, the applied characterization methods and their results are presented.

8.3.2 Composition, Thickness, and Topography of Ultrathin CMD Layers in Dry State: Characterization by ATR-FTIR, XPS, and AFM Measurements

Under dry conditions, the CMD-ut layers were characterized using ATR-FTIR, XPS, and AFM techniques. ATR-FTIR spectroscopy can be used to measure the infrared spectrum of thin layers deposited on the surface of an internal reflection

Table 8.1 Summary of the applied characterization techniques and the specific layer parameters obtained as measurement results

Analytical technique	Condition	Offered results
ATR-FTIR	Dry	Detection of carboxyl groups
XPS	Dry	Elemental composition, chemical states, thickness
SE	Dry	Lateral inhomogeneity, thickness, refractive index
AFM	Dry	Topography, surface roughness, thickness
CA meas.	Hydrated	Wettability, CA
OWLS	Hydrated	Refractive index, thickness, optical anisotropy, dry surface mass, protein-repellent ability
QCM-I	Hydrated	Viscoelastic parameters, hydrated surface mass, and thickness
Phase contrast microscopy	Hydrated	Cell-repellent ability

Adapted with permission from (Saftics 2018)

element the so-called ATR crystal. The sample layer absorbs infrared photons at certain wavelengths and attenuates the incident radiation through the evanescent field that is generated by the series of reflections on the crystal-layer interface. Graph A in Fig. 8.2 shows an ATR-FTIR spectrum of a CMD-ut-Am layer. The peaks at 1720–1740 cm^{-1} correspond to the characteristic stretching vibration of the carboxylic C=O groups of the grafted CMD (Zhang et al. 2005). This peak is also present in the bulk CMD at 1740 cm^{-1} (spectrum is not shown but can be found in our related paper (Saftics et al. 2016)).

XPS is used to measure the elemental composition of surfaces and thin layers by detecting the kinetic energy of photoelectrons ejected from the sample as a result of x-ray irradiation.

The goal of XPS measurements was the detection of CMD layers (by measuring changes in the elemental compositions and chemical states of elements) and determination of the thickness of CMD and silane layers under dry conditions. In contrast to aminosilane, epoxysilane does not contain distinctive heteroatom like N, and therefore the heteroatom-based thickness calculations could not be performed in case of CMD layers prepared with epoxysilane undercoating. Four types of sample wafers were measured to characterize the CMD-ut-Am layers, including bare Si, aminosilylated Si (Si/aminosilane), Si covered with CMD without aminosilane undercoating (Si/CMD, control sample), as well as aminosilylated Si covered with CMD (Si/aminosilane/CMD). Elemental compositions obtained on the examined samples can be seen in Fig. 8.2 B. In case of samples which were modified with aminosilane, a significant N signal could be observed. The Si/aminosilane/CMD samples presented particularly weakened signal of N, which was attributed to the covering effect of the CMD overlayer. Using the model that assumes an exponentially decaying probability of escaping a photoelectron with depth, the N signal provided the basis of determining the thickness of aminosilane and CMD layers (Rivière and Myhra 1998).

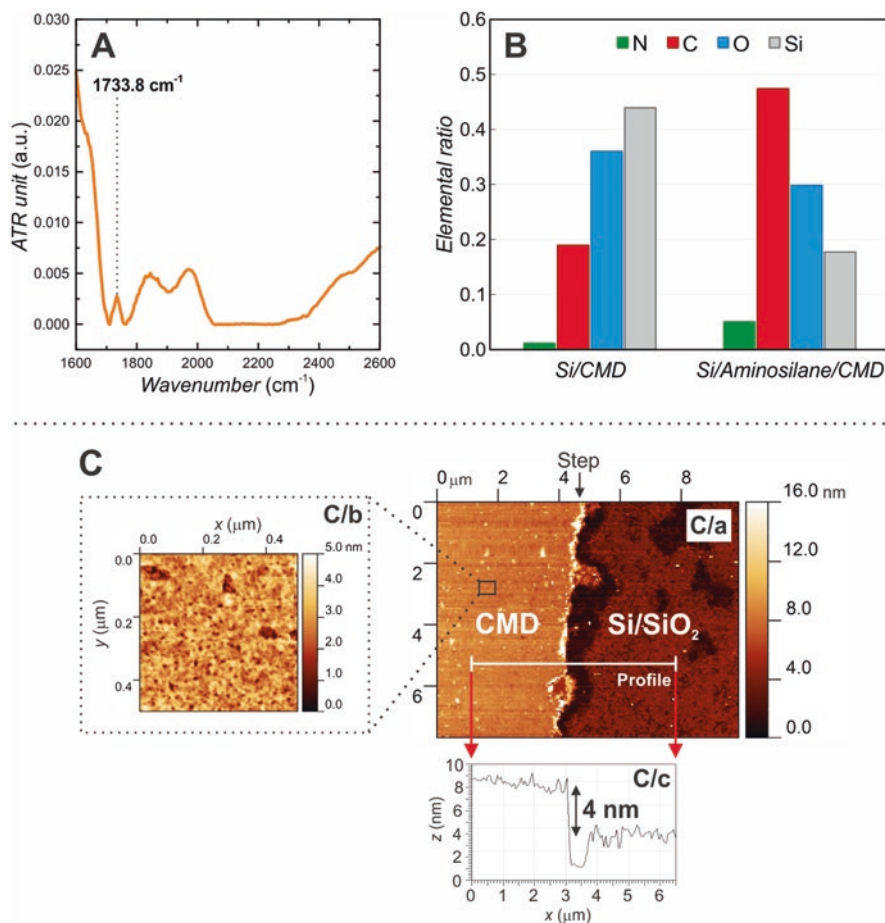


Fig. 8.2 Results on the characterization of CMD-ut layers under dry conditions. [Adapted with permission from (Saftics et al. 2016), copyright 2016 Elsevier]

(A) ATR-FTIR spectrum recorded on CMD-coated ATR crystal. The CMD-ut layer was grafted to the aminosilylated surface

(B) Elemental compositions of a CMD layer prepared without (sample Si/CMD) and with (sample Si/aminosilane/CMD) aminosilane undercoating

(C) AFM images about the surface of a CMD-ut-Am layer. **C/a**. The sample was prepared by gold lithography, resulting in a surface partially covered by the aminosilane/CMD coating, allowing to have a bare SiO₂ surface on the other half of the sample (10 \times 10 μm image). **C/b**. 0.5 \times 0.5 μm image representing the topography of CMD surface. Surface roughness RMS (root mean square) value of 1.1 nm was obtained, larger than the roughness value of native SiO₂ surface (0.2 nm), as expected. **C/c**. Height (z) profile of the aminosilane/CMD coating presented in image **C/a**

The thickness of the aminosilane layer was determined to be 2.30 nm. In case of control CMD samples, when the CMD was deposited onto a bare Si wafer without aminosilane, 0.07 nm was determined as the average thickness of CMD layer that means a weak partial coverage. This low value usually relates to slight

contaminations representing only some physically adsorbed CMD molecules. Nevertheless, grafting the CMD to aminosilane pre-coating provided 0.73 ± 0.10 nm CMD layer thickness (average \pm std., number of examined samples: six). According to this result, the aminosilane contributed to the efficient coupling of CMD to the surface that verifies the covalent grafting of CMD layer (Saftics et al. 2016).

AFM is a scanning probe microscopy technique that can be used for imaging surfaces at the nano- and micrometer level and for semiquantitative characterization of surfaces (e.g., measurement of surface roughness). Figure 8.2C presents AFM images captured on a CMD-ut-Am layer. The partly covered CMD sample was prepared using gold lithography. As a result, only the one-half of the Si wafer was coated with gold. After aminosilane and CMD grafting, the gold was removed allowing to achieve a sharp step between the aminosilane/CMD layer and uncoated Si (image C/a-b). Measuring the step heights, 3.2–5.8 nm (around 4 nm on the average) was determined for the total thickness of the covering layer (graph C/c). The resulting thickness of epoxysilane/CMD layers was in the same range. As the determined thickness corresponds to the combined thickness of the CMD and silane layer, the thickness of dry CMD coating itself should be below 4 nm. These findings are in good accordance with XPS measurements, which resulted in ca. 3.0 nm for the total thickness (2.30 nm aminosilane + 0.73 nm CMD) (Saftics et al. 2016).

It is worth highlighting that during the XPS and AFM measurements, the samples were kept in dry conditions. In this state, the CMD chains collapse and lie down on the surface forming a dense, very thin film. However, considering their real applications, CMD layers are applied in aqueous environments where they are in hydrated state. It is noted that in hydrating environments, CMD is able to swell up to even its multiple extent. Therefore, the characterization of CMD layers in their hydrated state is of high demand. For these examinations, *in situ* OWLS and QCM-I techniques were applied.

8.3.3 Nanostructure of Ultrathin CMD Layers Under Aqueous Conditions: Characterization by OWLS

Waveguide-based label-free optical biosensors detect refractive index changes occurring over the transducer surface. The sensing is performed by the evanescent field that is generated when the light inside the waveguide layer (that has the higher refractive index) is propagating by total internal reflections. The intensity of the reflected light, when meeting with the lower refractive index medium at the interface, extends over the interface into the medium generating an exponentially decaying (evanescent) electromagnetic field. Optical waveguide lightmode spectroscopy (OWLS) is a traditional setup of waveguide type biosensors. OWLS employs planar waveguides made of SiO₂-TiO₂ waveguide material where a zeroth-order waveguide mode (i.e., propagating standing electromagnetic wave) with two polarization states (transverse electric (TE) and transverse magnetic (TM) polarizations) is excited. The measurement of effective refractive index corresponding to the TE and TM waveguide modes enables one to determine the refractive index (n_A) and

thickness (d_A) of the examined adlayer using the 4-layer mode equations as evaluation model. The adlayer surface mass density (M_A , with a common dimension of ng/cm^2) can be calculated from the previously determined n_A and d_A utilizing the de Feijter's formula (De Feijter et al. 1978):

$$M_A = \frac{d_A (n_A - n_C)}{dn/dc} \quad (8.1)$$

where dn/dc is the refractive index increment of the analyte in its solution. In case of, e.g., proteins, a value of 0.182 mL/g is used (De Feijter et al. 1978). Regarding the calculation of n_A and d_A by the 4-layer mode equations, the classical and most commonly used model assumes a homogeneous and isotropic adlayer. In case of ordered adlayer structures, the optical anisotropy results in optical birefringence. When a material is birefringent, its apparent average refractive index can be decomposed into ordinary ($n_{A,o}$) and extraordinary refractive indices ($n_{A,e}$), and their ratio refers to the sign of birefringence. With the application of two waveguide modes, only d_A and the averaged n_A can be determined. However, it is still possible to characterize the ordered structure of the adlayer using the homogenous and isotropic model (Kovacs et al. 2013). Horvath and Ramsden pointed out (Horvath and Ramsden 2007) that the values of n_A and d_A can be used to decide whether the layer is optically isotropic or it has an ordered and anisotropic structure. Applying the 4-layer homogenous and isotropic model in case of an adlayer structure that is anisotropic (quasi-isotropic analysis), unrealistic n_A is observed meaning that the resulting n_A over- or underestimates the realistic (expected) adlayer n_A (Horvath and Ramsden 2007) (see Fig. 8.3A). When the adlayer is negatively birefringent (conformation of oriented molecules parallel with the surface) overestimated n_A ($n_{A,o} > n_{A,e}$), whereas the adlayer is positively birefringent (conformation of oriented molecules perpendicular to the surface) underestimated n_A can be detected ($n_{A,o} < n_{A,e}$) (Horvath and Ramsden 2007). As a result, the observed n_A is an indicator of adlayer birefringence. Also, the value of under- or overestimation is in relationship with the extent of anisotropy. Even in case of unrealistic n_A and d_A , the surface mass density can be still precisely determined owing to the error compensation of the de Feijter formula (Horvath and Ramsden 2007).

The in situ OWLS measurements were performed using a microfluidic assembly (flow-cell) that was mounted into the measurement head of the OWLS setup, and it was applied to maintain a continuous flow of solutions over the inserted sensor chip surface (Orgovan et al. 2014). The CMD grafting experiments monitored by OWLS were carried out on amino- and epoxysilylated SiO_2 - TiO_2 type sensor surfaces using different grafting solution pHs. The measured raw optical data (effective refractive indices of TE and TM modes (N_{TE} , N_{TM})) were evaluated by the homogenous isotropic 4-layer mode equations, providing the optical thickness (d_A) and apparent average refractive index (n_A) of the CMD-ut layer (De Feijter et al. 1978; Horvath and Ramsden 2007) and enabling to calculate the deposited surface mass density by the de Feijter formula.

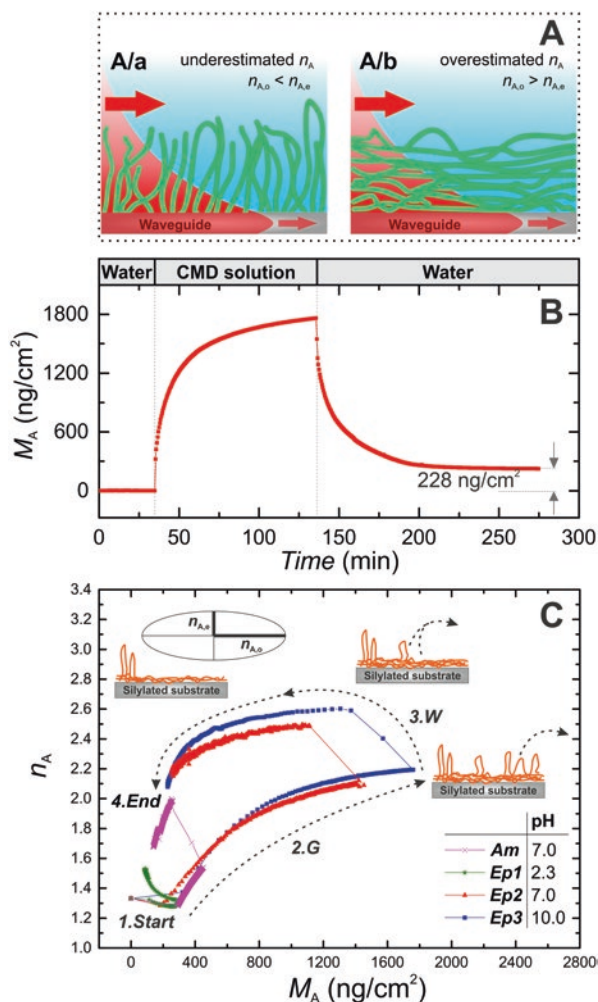


Fig. 8.3 OWLS measurement results obtained on the formation of CMD-ut layers. [Adapted with permission from (Saftics 2018) and from (Saftics et al. 2016), copyright 2016 Elsevier]

(A) Dependence of adlayer refractive index on different layer structures. In case of polymer chains perpendicular to the surface (C/a), positive birefringence, in case of chains parallel with the surface (C/b), negative birefringence can be observed by OWLS. The light propagating in the waveguide layer and its generated evanescent field over the surface are also shown

(B) Surface mass density (M_A) sensogram recorded during the deposition of CMD layer on an epoxysilylated OWLS sensor surface. The headers indicate the solutions flowed over the sample surface using a flow-cell

(C) Refractive index of CMD-ut layer as a function of deposited surface mass density. The curves represent different experimental conditions revealing the dependence of CMD layer structure during its formation on the applied silane precoating and pH of the grafting solution. The time-related direction of the measurements is indicated by the dashed arrows (*G* indicates the grafting, *W* the washing section of experiments). The inset table represents the different experimental conditions (*Am*, aminosilylated; *Ep*, epoxysilylated surfaces). The schemes above the curves illustrate the alteration of CMD layer nanostructure at the different experimental phases

Figure 8.3B The resulting mass curve of an in situ OWLS experiment revealing the kinetics of the formation of CMD-ut layer on an epoxysilylated OWLS chip surface. The stable signal that reached in the washing phase demonstrates the stability of the covalently grafted CMD layer. The surface mass of the CMD layer as well as the grafting efficiency was measured as the difference of mass values between the baseline and the end of the washing section

Our results revealing the alterations in the layers nanostructure throughout the grafting experiment as a function of deposited mass are presented in Fig. 8.3C. The conformation of CMD chains and thus the nanostructure was correlated with n_A values. As the realistic refractive index of hydrated dextran layers should be in the range of 1.36–1.52 (Piehler et al. 1999) (according to literature values), the obtained $n_A = 1.52$ – 2.21 values are clearly overestimated indicating a significant negative birefringence. Based on the quasi-isotropic analysis, the unrealistically high n_A values originate from mainly lying down CMD chains parallel with the surface. The n_A vs. M_A hysteresis curves of Fig. 8.3C help to understand the nanostructural alterations and layer formation mechanism by tracking the change of n_A originating from each added or removed CMD mass unit (Horvath et al. 2008, 2015; Escorihuela et al. 2015; Lee et al. 2015). The shown curves represent both the grafting (*G*) and washing (*W*) sections. The direction of the experiment is indicated by the dashed arrows, and the illustrations correspond to the supposed layer nanostructure at the given experimental section. We found that the nanostructure and amount (mass) of CMD layers significantly varied depending on the applied grafting conditions: the pH of grafting solution and grafting chemistry (type of silane coating).

Based on the high n_A values, it was observed that under neutral and alkalic conditions (pH 7.0 and 10.0), the conformation of CMD chains was dominantly parallel with the surface. Regarding the formation process, n_A was increasing during the grafting section and when the washing section started, n_A further increased indicating that first the weakly bound brush-like molecules were removed from the surface. Subsequently, in the washing section, CMD chains with lain down orientation were also desorbed; however the rate of their removal and the removed amount was smaller. The mechanism of CMD layer formation was significantly different at pH 2.3. In this case, the relative amount of lain down molecules was smaller which was supported by the n_A values (1.52) close to the realistic CMD refractive index. In the grafting section, the deposition of loops was predominant, and as a result, $n_A \approx 1.30$ was calculated at the end of the grafting phase. This refers to a layer composed of randomly oriented chains.

Nevertheless, the chains extending toward the solution were easily removed in the subsequent washing process, and finally, chains mainly with lain down conformations remained on the surface. The dependence of the CMD layer structure upon the pH on epoxysilylated surfaces is supposed to derive from the pH-dependent yield of the grafting reaction (reaction between epoxide and carboxyl/hydroxyl functions).

In case of the experiments performed on aminosilylated surfaces (pH 7.0), the shape of n_A vs. M_A curves was similar to those measured on epoxytated surfaces under neutral and basic conditions. However, as the increase of n_A was smaller, a more extended layer was assumed. This result obtained on the aminated surface suggested that compared to layers prepared on epoxytated surfaces at pH 7.0 and 10.0, the CMD was attached via smaller number of surface grafting points.

8.3.4 Viscoelastic Properties of Ultrathin CMD Layers: Characterization by QCM

We applied the QCM technique to reveal the viscoelastic properties of hydrated CMD-ut layers throughout the whole layer formation event. QCM is a label-free biosensor that applies mechanical transduction principle for sensing and for characterizing thin coatings. A QCM sensor chip is composed of a resonant piezoelectric quartz crystal disk contacted on its both sides with planar gold electrodes. The AC voltage applied on the electrodes generates shear oscillation in the piezoelectric crystal at its fundamental resonance frequency (5 MHz) and also at overtone frequencies. The oscillation results in a standing plane wave¹ (also known as acoustic wave), which vertically propagates through the crystal and penetrates into the medium over the crystal surface (Ferreira et al. 2009; Johannsmann 2015). As added mass on the sensor surface detunes the resonance frequencies (f_n , where n is the overtone number), QCM can measure the mass of deposited layers by recording the shift in the quartz crystal' resonance frequencies (Δf_n). When the added mass is not rigid and it has significant viscoelasticity (which is common in case of soft and hydrated biomaterial films (Ismail et al. 1996; Marx 2003; Laos et al. 2006; Kittle et al. 2011)), it also changes the decay characteristic of the penetrating wave. The decay characteristic is in connection with the energy dissipation of the oscillation that can be quantified by the dissipation factor (D_n or ΔD_n , measured for fundamental and each overtone frequency as well), and it can provide results on the adlayer viscoelastic properties. Moreover, QCM is also sensitive to the mass of solvent molecules coupled to the adlayer enabling to measure the hydrated mass. As viscoelastic properties and hydration cannot be measured by optical methods, these features make QCM unique among the surface analytical techniques.

Two models are mostly used for evaluating the measured Δf_n and ΔD_n data. The simplest model, the Sauerbrey equation does not take dissipation (and viscoelasticity) into account and presumes that the surface mass density (M_A) is a linear function of the measured normalized frequency shift ($\Delta f_n/n$) (Sauerbrey 1959):

$$\Delta M = -C \frac{\Delta f_n}{n} \quad (8.2)$$

¹This principle is analogous to the measurement principle of evanescent field applying sensors, where a standing electromagnetic field over the waveguide layer is generated allowing to sense analytes.

where C refers to the mass sensitivity constant that depends on the quartz crystal physical properties.

In case of highly solvated adlayers presenting viscoelastic properties, the Sauerbrey equation is not valid. The quantitative evaluation requires to consider the layer viscoelastic behavior and continuum mechanical models, most commonly the Voigt-Kelvin model should be used. The most commonly applied implementation of this viscoelastic model was published by Voinova and co-workers, and it is usually referred as Voinova's equations (Voinova et al. 1999). The data evaluation is based on the simultaneous error-minimizing fit of the measured Δf_n and ΔD_n data with the model equations. The fit results in the thickness (d_A), shear viscosity (η_A), as well as shear elastic modulus (μ_A) of the formed adlayer, supposing a known layer mass density (ρ_A) (Voinova et al. 1999; Höök et al. 2001; Stengel et al. 2005). In case of layers made of heavily hydrated polymers, such as CMD, an approximation of 1000 kg/m^3 can be used for the value of ρ_A (Müller et al. 2005).

We used the QCM-I method (MicroVacuum Ltd., Budapest, Hungary) that employs impedance analysis for reading out frequency and dissipation data (QCM-I denotes QCM with impedance analysis). Similarly to OWLS, the in situ setup applies a flow-cell assembled in the measurement head and mounted on the sensor surface. The continuous (real-time) monitoring of surface events is achieved by the sequential measurement of impedance spectra enabling to obtain f_n and D_n data simultaneously at each measurement time. The in situ QCM experiments were performed with the same solution flow sections as in case of OWLS. The data analysis (model fit) was carried out using a home-developed evaluation program.

Our results obtained from in situ QCM-I measurements on the formation of CMD-ut-Am layers are shown in Fig. 8.4. The analysis of $\Delta f_n/n$ and ΔD_n data (graph **A** and **B**) can provide useful qualitative information about the layer. While the environmental noise can significantly disturb the penetrating acoustic wave at the fundamental resonance frequency (Dutta and Belfort 2007) ($n = 1$), only data for overtones $n > 1$ ($n = 3, 5, 7$) were considered. As it can be seen from the significant shifts in $\Delta f_n/n$ and ΔD_n data, large amount of CMD was deposited in the grafting section; however, the washing strongly affected the layer and a large amount of CMD was washed off. Besides the CMD amount, the viscoelastic properties also changed in the washing section indicated by the dissipation, which turned from a strongly dissipative state ($\Delta D_3 = 60 \times 10^{-6}$) to less dissipative (4.8×10^{-6}). It can be assumed that a soft CMD layer formed during the grafting section; however, the loosely bound chains desorbed, and a thin CMD coverage remained. The adequacy of the application of Sauerbrey equation for evaluation was checked based on the magnitude of ΔD_n data. If ΔD_n exceeds the critical value of 2×10^{-6} , the layer cannot be treated to be rigid, and the Sauerbrey relationship is not valid (Vogt et al. 2004; Liu et al. 2011). The large values of ΔD_n ($\Delta D_3 = 4.8 \times 10^{-6}$) indicated a viscoelastic case; therefore Voinova's equations implemented in our home-developed code were used for the evaluation and quantification of layer properties. Δf_n and ΔD_n data obtained from fitting the measured curves are shown in Fig. 8.4, and as it can be seen, good fit quality could be achieved. The thickness ($d_A^{\text{QCM,V}}$), surface

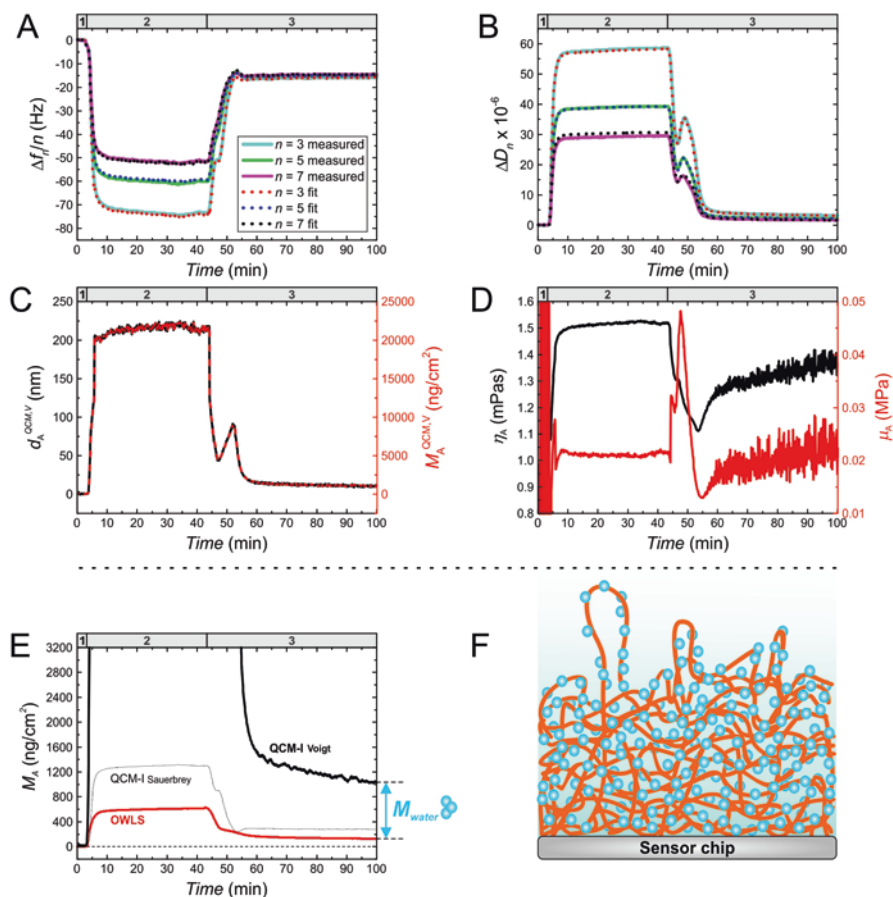


Fig. 8.4 QCM-I results measured on the formation of CMD-ut-Am nanolayers. [Adapted with permission from (Saftics et al. 2018), copyright 2018 Springer Nature Publishing AG, used under CC BY 4.0]

(A, B) Normalized frequency shift (A) and dissipation shift (B) data measured by QCM-I over the time of CMD-ut-Am layer formation on SiO₂-TiO₂ surfaces. The data correspond to the overtones $n = 3, 5, 7$. The in situ monitored experiments were carried out in three consecutive phases of solution flows as follows (shown by the header numbers): flow of polymer-free water to reach a stable baseline (1), polymer solution flow (2), and water flow applied to wash the weakly adsorbed molecules. Fitted curves of the measured $\Delta f_n/n$ and ΔD_n data using the Voigt-based viscoelastic model are also shown

(C) Full thickness and mass plots indicated by solid black as well as dashed red curves, respectively. The mass was simply proportional with the thickness by the value of layer density ($\rho_A = 1000 \text{ kg/m}^3$)

(D) Shear viscosity (black) and shear elastic modulus (red) curves calculated using the Voigt-based model

(E) Surface mass density measured by OWLS (solid red line) and QCM-I (solid black line). The thicker black line indicates the mass calculated by the Voigt-based model, the thinner black line refers to the third overtone mass calculated by the Sauerbrey equation. M_{water} indicates the mass of coupled water

(F) The illustration represents the final structure of the formed CMD-ut-Am layer together with coupled water molecules

Table 8.2 Summary of parallel OWLS and QCM-I results measured on CMD-ut layers: main physical properties and their comparison with literature values

	Measured	References
	CMD	PLL-g-D ^c , D ^d , CMC ^c
M_A^{OWLS} (ng/cm ²)	124 ± 23	–
$M_A^{\text{QCM,S3}}$ (ng/cm ²)	277 ± 28	–
$M_A^{\text{QCM,V}}$ (ng/cm ²)	1102 ± 487	–
φ_A (%)	89	57 ^c (Nalam et al. 2013), 60–70 ^c (Perrino 2009)
n_A	1.66 ± 0.22	–
d_A^{OWLS} (nm)	0.9 ± 0.5	–
$d_A^{\text{QCM,S3}}$ (nm)	2.8 ± 0.3	–
$d_A^{\text{QCM,V}}$ (nm)	11.0 ± 4.9	–
η_A (mPa·s)	1.43 ± 0.27	0.50 ± 0.26 ^d (Kuhner and Sackmann 1996)
μ_A (MPa)	0.03 ± 0.01	0.1–0.2 ^c (Liu et al. 2011)

The data are presented as averaged values ± standard deviations calculated from three repeated experiments. The data represent the remained and stably grafted layers reached at the end of washing section. The superscript indications refer to the following: ^a, the reference data correspond to different polymers; ^b, obtained on PLL-g-D (D as dextran); ^c, on dextran (D); as well as ^d, on carboxymethyl cellulose (CMC)

M_A^{OWLS} , surface mass density recorded by OWLS; $M_A^{\text{QCM,S3}}$, $M_A^{\text{QCM,V}}$, surface mass density recorded by QCM-I and evaluated using the Sauerbrey model or Voigt-based model, respectively; φ_A , hydration degree; n_A , d_A^{OWLS} , refractive index, as well as optical thickness of CMD adlayer obtained by OWLS; $d_A^{\text{QCM,S3}}$, $d_A^{\text{QCM,V}}$, thickness of CMD adlayer obtained by QCM-I and evaluated using the Sauerbrey equation or Voigt-based model, respectively; η_A , μ_A , shear viscosity and shear elastic modulus of CMD adlayer, calculated using the Voigt-based model. References are designated as shown

Adapted with permission from (Saftics et al. 2018), copyright 2018 Springer Nature Publishing AG, used under CC BY 4.0

mass density ($M_A^{\text{QCM,V}}$), and viscoelastic data (η_A , μ_A) calculated by the fits are shown in Fig. 8.4. The resulting data representing the remained stable layer after washing are presented in Table 8.2. Herein, literature data about similar layers are also shown to provide a basis for comparison (Saftics et al. 2018).

8.3.5 Hydration Properties of Ultrathin CMD Layers: Combining QCM and OWLS Results

As a consequence of the lack of individual analytical techniques capable of measuring heavily hydrated objects at the nanometer scale, the nanostructure and dynamic behavior of ultrathin layers in aqueous environment is still poorly characterized. A main limitation of the optical techniques is that water molecules, coupled to the layer, cannot be distinguished from the aqueous background (bulk phase), and therefore they do not provide change in the refractive index signal.

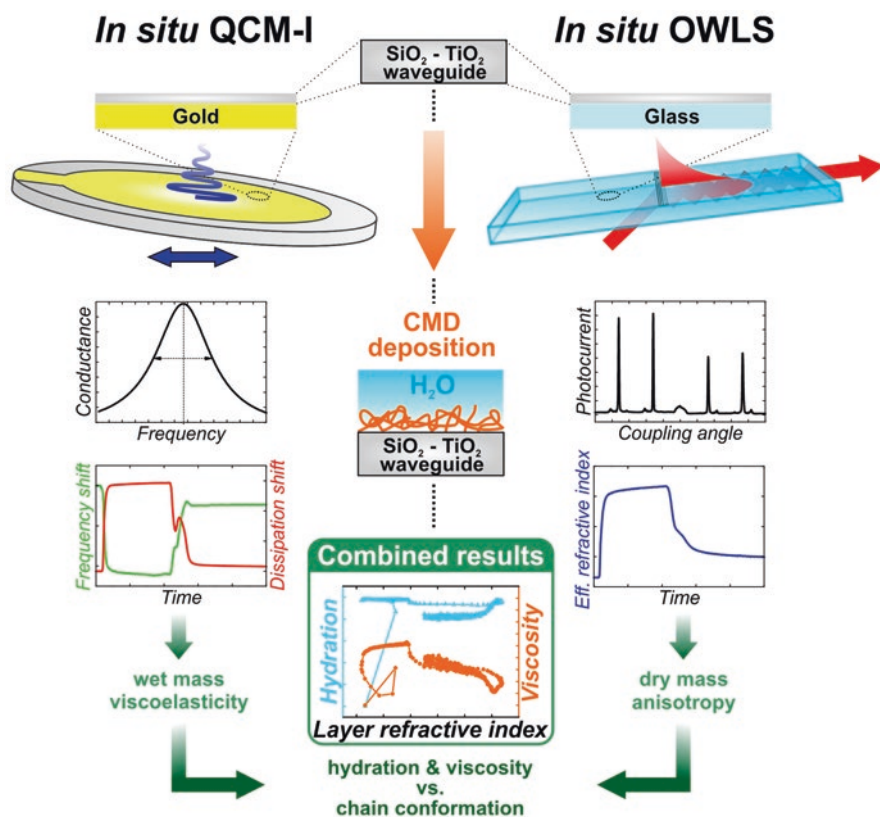


Fig. 8.5 Scheme about the methodology applied for exploring the formation as well as hydration and nanostructure of ultrathin CMD layers using parallel in situ OWLS and QCM-I measurements. We used chemically identical substrate surfaces in both measurement techniques. [Adapted with permission from (Saftics et al. 2018), copyright 2018 Springer Nature Publishing AG]

Consequently, only the “dry” mass of an analyte layer can be measured (Höök et al. 2002; Vörös 2004). In contrast to OWLS, QCM is sensitive to solvent molecules coupled to the layer, since it measures all the masses oscillating with the crystal. This combined “wet” mass cannot be uncoupled to the mass of dry adlayer and mass of bound solvent molecules. However, the combination of OWLS and QCM provides a special tool to determine the hydration degree of nanolayers (φ_A) by utilizing both the optical (“dry” OWLS mass, M_A^{OWLS}) and mechanical (“wet” QCM-I Voigt mass, M_A^{QCM}) mass data (Höök et al. 2001, 2002; Vörös 2004; Müller et al. 2005). A scheme of the combined evaluation methodology is shown in Fig. 8.5.

The dry and wet surface mass density values as a function of time measured during the formation of a CMD-ut-Am layer are plotted in Fig. 8.4E (specific mass data corresponding to the remained stable layer are shown in Table 8.2). The difference

between the dry and wet mass, highlighted by M_{water} , refers to the mass of water molecules coupled to the CMD layer. The hydration degree (φ_A) of the stable layer was determined to be 89%. An assumed structure of the remained stable layer including coupled water molecules is also shown (F).

The combination of OWLS and QCM-I data also enabled us to characterize the layer nanostructure in terms of hydration and viscosity (see Fig. 8.5). We found that the conformational rearrangement during the washing accompanied with significant change in the layer hydration and viscosity. For more details see our related publication (Saftics et al. 2018).

8.3.6 Thickness and Composition of Spin-Coated and Crosslinked CMD Layers: Characterization by Ellipsometry and XPS

Spectroscopic ellipsometry is an optical technique that measures the polarization state of light reflected from the sample in order to measure the optical properties and thickness of the constituting layers. The wavelength spectra of the so-called ellipsometric angles (Ψ and Δ , characterizing the polarization state) are evaluated based on the fit of an adequate optical model, which is a function of the structure and physical parameters of the sample.

Ellipsometry could be effectively used to characterize the CMD-sc layers and determine their thickness and refractive index. It is important to emphasize that the thickness of these layers was over 10 nm. Below this value, in case of few nanometers thick CMD-ut coatings, CMD could not be separated from the substrate, and therefore, reliable layer parameters could not be determined. In order to control the thickness, the CMD-sc layers were fabricated with applying different spin-coating rotational speeds. Mapping mode spectroscopic ellipsometry measurements were performed to obtain thickness and refractive index maps about the examined samples. We developed an ellipsometric optical model that could be effectively used for the evaluation of the measured Ψ and Δ spectra with the main goal of determining the thickness of dry CMD-sc layers.

The calculations were performed in the 450–900 nm wavelength range. The refractive indices corresponding to the different layers were modeled using the Cauchy's equation. Fitted Ψ and Δ spectra of a measured CMD-sc sample (A) and evaluation results (C, D, and E) can be seen in Fig. 8.6, where details of the used optical model developed for the specific evaluations are also shown (B). The model presumes vertically inhomogeneous (gradient) refractive index in the SiO_2 - TiO_2 waveguide layer which was divided into five slices with increasing refractive indices in depth. This presumption was based on the expectation that the density of the layer from the bottom to the top was decreased by the standard acidic cleaning applied on the OWLS sensor chips. The wavelength dependence of CMD refractive index characterized by the B parameter was determined in separate measurements. For these measurements, the CMD layers were spin-coated on gold substrates,

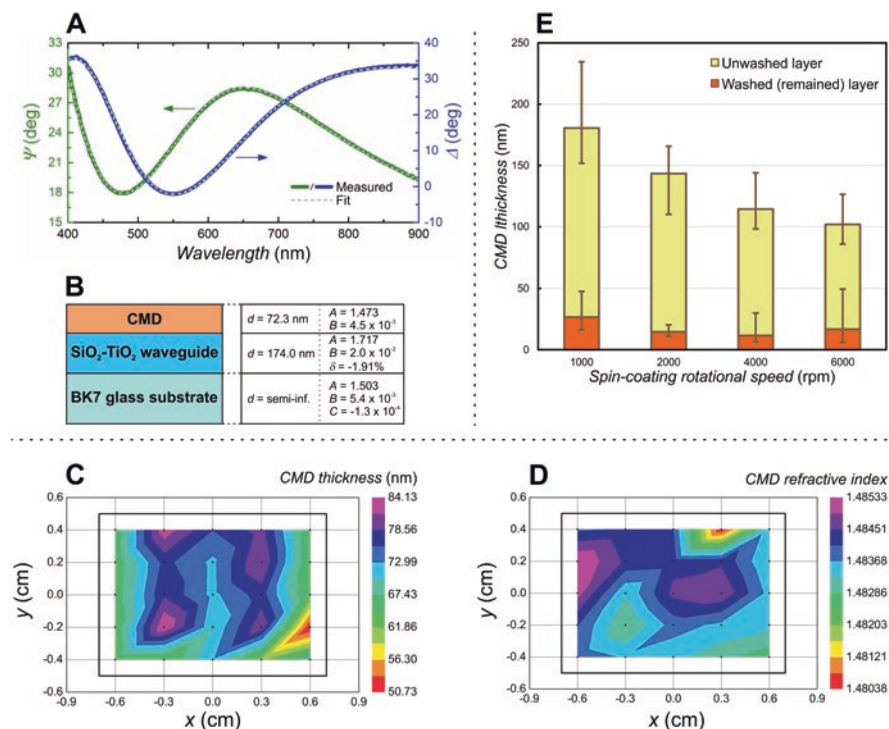


Fig. 8.6 Ellipsometry results obtained on CMD-sc layers. [Adapted with permission from (Saftics 2018) and from (Saftics et al. 2019), copyright 2019 American Chemical Society]

(A) Ψ and Δ spectra recorded on a CMD-sc layer that was prepared on an OWLS model substrate. The measured and fitted spectra are indicated by the solid and dashed lines, respectively (MSE = 1.9). The spectra correspond to the center of the measured sample (applied spin-coating rotational speed: 6000 rpm)

(B) Optical model and results obtained from the fit that is presented in graph A (the shown parameters are the following: d , thickness; A, B, C , parameters of Cauchy's equation; vertical inhomogeneity degree of the layer (δ))

(C, D) Lateral maps about thickness (d_{CMD}) and refractive index ($n_{\text{CMD}, 632.8 \text{ nm}}$) of the CMD layer. The refractive index was calculated using the Cauchy's equation at the wavelength of 632.8 nm

(E) Thickness of CMD-sc layers depending on the applied rotational speeds. The yellow-colored (top) columns refer to the thickness of CMD layers as prepared (unwashed). The orange (bottom) columns refer to the thickness of CMD layers remaining after the washing

where improved optical contrast and sensitivity could be achieved. As a result, $B_{\text{CMD}} = 4.5 \times 10^{-3} \pm 7.4 \times 10^{-4}$ was found (average \pm std., four analyzed samples) (Saftics et al. 2017).

Graphs C and D show the evaluated thickness and refractive index maps of an unwashed CMD-sc sample. The thickness values depending on the spin-coating rotational speeds both for unwashed and washed samples are presented in bar chart E. The rotational speed significantly affected the unwashed CMD layer thickness, and the effect followed the expected tendency. However, the effect of varying

rotational speeds on the thickness of remained layers was not obvious. It was observed that the washing removed 80% of the CMD thickness resulting in 10–50 nm thickness for the remained layers (Saftics et al. 2019).

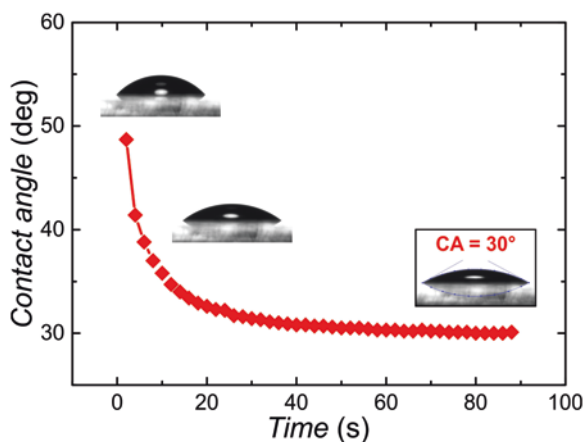
XPS was used to determine the elemental composition of CMD-sc layers with the main goal of phosphorous (P) detection in order to determine the crosslinking degree. Due to the fact that STMP crosslinker molecules were the only P-containing compounds, the determination of P could be used to detect the presence of crosslinks and measure their relative amount. As a result, the determined $0.2\text{--}0.4 \pm 0.1\%$ P content should correspond to an approx. 5% crosslinking degree (Saftics et al. 2019).

8.3.7 Wetting Properties of Spin-Coated and Crosslinked CMD Layers Characterized by Contact Angle Measurements

Measuring the CA of water droplets deposited on surfaces can be used to characterize the wettability and hydrophilic-hydrophobic nature (energetics) of a surface. Due to the fact that hydrogels can absorb a large amount of water, dynamic CA measurements are useful in demonstrating the hydrogel nature of the examined layer.

Figure 8.7 presents the results of CA measurements on CMD-sc surfaces. Compared to the aminosilane-coated surface (A), the CMD-sc layer (B) significantly affected the CA, resulting in CAs in the range of 10–30° (with respect to multiple samples). According to our observations, the drop shape remarkably varied in time after deposition on CMD-sc surface. The phenomenon was analyzed by dynamic CA measurements, and a typical outcome is shown in graph C. It was found that the CA continuously decreased until relaxation. The drop in CA can be attributed to a significant water uptake which characteristic is typical for hydrogels.

Fig. 8.7 Water CAs measured on a CMD-sc sample. [Adapted with permission from (Saftics et al. 2019), copyright 2019 American Chemical Society]
The graph shows the continuous change of CA in time, presenting the dynamic wetting behavior of the CMD-sc layer and its hydrogel nature.



It should be noted that such dynamic behavior was not detected for CMD-ut layers, which is an obvious verification of the difference (thickness, crosslinking) between the developed CMD-ut and CMD-sc layers (Saftics et al. 2019).

8.3.8 Protein- and Cell-Repellent Ability Characterized by OWLS and Phase Contrast Microscopy

A primary goal of the fabrication of CMD layers on SiO₂-TiO₂-type optical biosensor surfaces was the development of biofunctional sensor coatings with advanced antifouling abilities.

We applied the in situ OWLS method to characterize the protein-repellent (NSB-resistant) ability of CMD-ut and CMD-sc layers by measuring the amount (surface mass density) of adsorbed proteins. In these experiments, three different protein molecules with varying isoelectric point (pI) and molecular weight values were tested, including bovine serum albumin (BSA), fibrinogen (FGN), and lysozyme (LYZ). Typical adsorption curves measured on CMD-ut and CMD-sc surfaces are shown in Fig. 8.8A/a and A/b, respectively. Compared to the control measurements performed on bare SiO₂-TiO₂ surfaces, it is obvious that the CMD layers suppressed the adsorbed amount of each protein. The slightly higher deposited mass values of LYZ can be attributed to the attraction of positively charged LYZ (pI = 11.0) to the negatively charged CMD molecules (pK_a ≈ 3) (Sidobre et al. 2002) in the used buffer environment (phosphate-buffered saline (PBS), pH 7.4) (Saftics et al. 2019).

The cell-repellent ability of CMD layers was tested by adhesion experiments using living HeLa cells, and the adhesion was observed by phase contrast microscopy. As shown in Fig. 8.8B, the presence of CMD provided considerable resistance against cell adhesion.

8.4 Summary

In this chapter, we have presented the surface analytical methodologies we applied to reveal the properties of our developed thin CMD layers. The proposed biosensor applications, for which the CMD layers were fabricated, demand to understand the layer structure and behavior in aqueous environment. Although the number of applicable techniques is very limited and there is no such method that could provide a full layer characterization, we demonstrated that using a collection of highly sensitive surface analytical techniques, several characteristics can be understood. It has been shown that the OWLS and QCM methods are capable to provide unique structural and mechanical data about heavily hydrated nanolayers. The presented measurement and data analysis methodologies are proposed to facilitate the analysis of biosensor coatings or other hydrated thin coatings used in various fields.

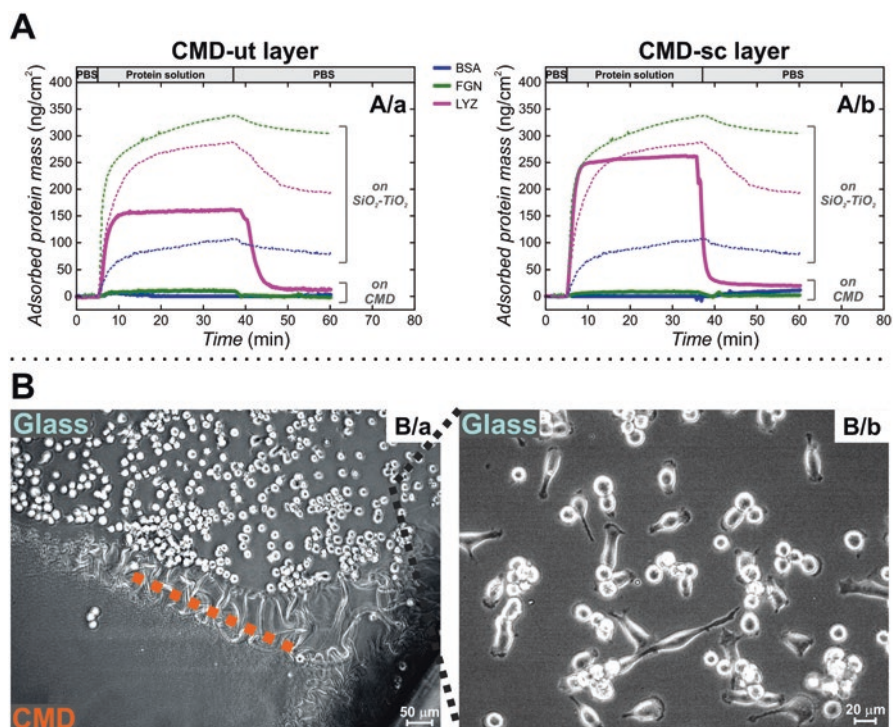


Fig. 8.8 Protein- and cell-repellent ability of CMD layers. [Adapted with permission from (Saftics 2018) and (Saftics et al. 2019), copyright 2019 American Chemical Society]

(A) Adsorbed mass of BSA, FGN, and LYZ proteins in situ monitored by OWLS. Graph A/a and A/b represent measurements performed on CMD-ut and CMD-sc layers, respectively. The different curve colors designate the specific proteins. While the solid curves were obtained on CMD-covered surfaces, the dashed ones indicate measurements carried out on unmodified SiO₂-TiO₂ substrate surfaces. The experimental phases are shown by the graph headers

(B) Image B/a corresponds to a sample partially coated with CMD-sc layer as indicated by the dashed line. While cells did not adhere on CMD surface, they could adhere on glass (see image B/b taken on glass surface). The images were captured after 4 (B/a) and 6 (B/b) hours of incubation in cell culture

Acknowledgments This study was funded by the Momentum (“Lendület”) Program of the Hungarian Academy of Sciences, the National Research, Development and Innovation Office (NKFIH) [ERC_HU, KKP_19, KH and FK-128901 Programs] and János Bolyai Research Scholarship of the Hungarian Academy of Sciences are also gratefully acknowledged.

References

- Akkoyun A, Bilitewski U (2002) Optimisation of glass surfaces for optical immunosensors. *Biosens Bioelectron* 17:655–664. [https://doi.org/10.1016/S0956-5663\(02\)00029-5](https://doi.org/10.1016/S0956-5663(02)00029-5)
- Balakrishnan B, Banerjee R (2011) Biopolymer-based hydrogels for cartilage tissue engineering. *Chem Rev* 111:4453–4474. <https://doi.org/10.1021/cr100123h>

- Chandra P (ed) (2016) *Nanobiosensors for personalized and onsite biomedical diagnosis*. Institution of Engineering and Technology, London
- Chandra P, Tan YN, Singh SP (2017) *Next generation point-of-care biomedical sensors technologies for cancer diagnosis*. Springer, Singapore
- Cutionco MFA, Tan MH, Ng MYK et al (2014) Composite pullulan–dextran polysaccharide scaffold with interfacial polyelectrolyte complexation fibers: A platform with enhanced cell interaction and spatial distribution. *Acta Biomater* 10:4410–4418. <https://doi.org/10.1016/j.actbio.2014.06.029>
- De Feijter J, Benjamins J, Veer F (1978) Ellipsometry as a tool to study the adsorption behavior of synthetic and biopolymers at the air water interface. *Biopolymers* 17:1759–1772. <https://doi.org/10.1002/bip.1978.360170711>
- Dutta AK, Belfort G (2007) Adsorbed gels versus brushes: viscoelastic differences. *Langmuir* 23:3088–3094. <https://doi.org/10.1021/la0624743>
- Elam JH, Nygren H, Stenberg M (1984) Covalent coupling of polysaccharides to silicon and silicon rubber surfaces. *J Biomed Mater Res* 18:953–959. <https://doi.org/10.1002/jbm.820180809>
- Elender G, Kühner M, Sackmann E (1996) Functionalisation of Si/SiO₂ and glass surfaces with ultrathin dextran films and deposition of lipid bilayers. *Biosens Bioelectron* 11:565–577. [https://doi.org/10.1016/0956-5663\(96\)83292-1](https://doi.org/10.1016/0956-5663(96)83292-1)
- Escorihuela J, González-Martínez MÁ, López-Paz JL et al (2015) Dual-polarization interferometry: a novel technique to light up the nanomolecular world. *Chem Rev* 115:265–294. <https://doi.org/10.1021/cr5002063>
- Ferreira L, Rafael A, Lamghari M et al (2004) Biocompatibility of chemoenzymatically derived dextran-acrylate hydrogels. *J Biomed Mater Res* 68A:584–596. <https://doi.org/10.1002/jbm.a.20102>
- Ferreira GNM, Da-Silva A-C, Tomé B (2009) Acoustic wave biosensors: physical models and biological applications of quartz crystal microbalance. *Trends Biotechnol* 27:689–697. <https://doi.org/10.1016/j.tibtech.2009.09.003>
- Höök F, Kasemo B, Nylander T et al (2001) Variations in coupled water, viscoelastic properties, and film thickness of a Mefp-1 protein film during adsorption and cross-linking: a quartz crystal microbalance with dissipation monitoring, ellipsometry, and surface plasmon resonance study. *Anal Chem* 73:5796–5804. <https://doi.org/10.1021/ac0106501>
- Höök F, Vörös J, Rodahl M et al (2002) A comparative study of protein adsorption on titanium oxide surfaces using in situ ellipsometry, optical waveguide lightmode spectroscopy, and quartz crystal microbalance/dissipation. *Colloids Surf B Biointerfaces* 24:155–170. [https://doi.org/10.1016/S0927-7765\(01\)00236-3](https://doi.org/10.1016/S0927-7765(01)00236-3)
- Horvath R, Ramsden JJ (2007) Quasi-isotropic analysis of anisotropic thin films on optical waveguides. *Langmuir* 23:9330–9334. <https://doi.org/10.1021/la701405n>
- Horvath R, McColl J, Yakubov GE, Ramsden JJ (2008) Structural hysteresis and hierarchy in adsorbed glycoproteins. *J Chem Phys* 129:071102. <https://doi.org/10.1063/1.2968127>
- Horvath R, Gardner HC, Ramsden JJ (2015) Apparent self-accelerating alternating assembly of semiconductor nanoparticles and polymers. *Appl Phys Lett* 107:041604. <https://doi.org/10.1063/1.4927403>
- Ismail IM, Gray ND, Owen JR (1996) A QCM analysis of water absorption in lithium polymer electrolytes. *J Chem Soc Faraday Trans* 92:4115. <https://doi.org/10.1039/ft9969204115>
- Johannsmann D (2015) *The quartz crystal microbalance in soft matter research*. Springer, Cham
- Kittle JD, Du X, Jiang F et al (2011) Equilibrium water contents of cellulose films determined via solvent exchange and quartz crystal microbalance with dissipation monitoring. *Biomacromolecules* 12:2881–2887. <https://doi.org/10.1021/bm200352q>
- Knoll W (ed) (2013) *Handbook of biofunctional surfaces*, 1st edn. Pan Stanford Publishing, Boca Raton
- Kovacs N, Patko D, Orgovan N et al (2013) Optical anisotropy of flagellin layers: in situ and label-free measurement of adsorbed protein orientation using OWLS. *Anal Chem* 85:5382–5389. <https://doi.org/10.1021/ac3034322>

- Kuhner M, Sackmann E (1996) Ultrathin hydrated dextran films grafted on glass: preparation and characterization of structural, viscous, and elastic properties by quantitative microinterferometry. *Langmuir* 12:4866–4876. <https://doi.org/10.1021/la960282+>
- Laos K, Parker R, Moffat J et al (2006) The adsorption of globular proteins, bovine serum albumin and β -lactoglobulin, on poly-L-lysine–fucellaran multilayers. *Carbohydr Polym* 65:235–242. <https://doi.org/10.1016/j.carbpol.2006.01.010>
- Lee MH, Boettiger D, Composto RJ (2008) Biomimetic carbohydrate substrates of tunable properties using immobilized dextran hydrogels. *Biomacromolecules* 9:2315–2321. <https://doi.org/10.1021/bm8002094>
- Lee T-H, Hirst DJ, Aguilar M-I (2015) New insights into the molecular mechanisms of biomembrane structural changes and interactions by optical biosensor technology. *Biochim Biophys Acta Biomembr* 1848:1868–1885. <https://doi.org/10.1016/j.bbame.2015.05.012>
- Lian M, Chen X, Lu Y, Yang W (2016) Self-assembled peptide hydrogel as a smart biointerface for enzyme-based electrochemical biosensing and cell monitoring. *ACS Appl Mater Interfaces* 8:25036–25042. <https://doi.org/10.1021/acsami.6b05409>
- Linder V, Gates BD, Ryan D et al (2005) Water-soluble sacrificial layers for surface micromachining. *Small* 1:730–736. <https://doi.org/10.1002/sml.200400159>
- Liu Z, Choi H, Gatenholm P, Esker AR (2011) Quartz crystal microbalance with dissipation monitoring and surface plasmon resonance studies of carboxymethyl cellulose adsorption onto regenerated cellulose surfaces. *Langmuir* 27:8718–8728. <https://doi.org/10.1021/la200628a>
- Liu J, Qi C, Tao K et al (2016) Sericin/dextran injectable hydrogel as an optically trackable drug delivery system for malignant melanoma treatment. *ACS Appl Mater Interfaces* 8:6411–6422. <https://doi.org/10.1021/acsami.6b00959>
- Liu M, Zeng X, Ma C et al (2017) Injectable hydrogels for cartilage and bone tissue engineering. *Bone Res* 5:17014. <https://doi.org/10.1038/boneres.2017.14>
- Löfås S, Johnsson B (1990) A novel hydrogel matrix on gold surfaces in surface plasmon resonance sensors for fast and efficient covalent immobilization of ligands. *J Chem Soc Chem Commun*:1526–1528. <https://doi.org/10.1039/C39900001526>
- Löfås S, Johnsson B, Tegendal K, Rönnberg I (1993) Dextran modified gold surfaces for surface plasmon resonance sensors: immunoreactivity of immobilized antibodies and antibody-surface interaction studies. *Colloids Surf B Biointerfaces* 1:83–89. [https://doi.org/10.1016/0927-7765\(93\)80038-Z](https://doi.org/10.1016/0927-7765(93)80038-Z)
- Löfås S, Johnsson B, Edström Å et al (1995) Methods for site controlled coupling to carboxymethyl-dextran surfaces in surface plasmon resonance sensors. *Biosens Bioelectron* 10:813–822. [https://doi.org/10.1016/0956-5663\(95\)99220-F](https://doi.org/10.1016/0956-5663(95)99220-F)
- Marx KA (2003) Quartz crystal microbalance: a useful tool for studying thin polymer films and complex biomolecular systems at the solution–surface interface. *Biomacromolecules* 4:1099–1120. <https://doi.org/10.1021/bm020116i>
- Massia SP, Stark J, Letbetter DS (2000) Surface-immobilized dextran limits cell adhesion and spreading. *Biomaterials* 21:2253–2261. [https://doi.org/10.1016/S0142-9612\(00\)00151-4](https://doi.org/10.1016/S0142-9612(00)00151-4)
- Mateescu A, Wang Y, Dostalek J, Jonas U (2012) Thin hydrogel films for optical biosensor applications. *Membranes (Basel)* 2:40–69. <https://doi.org/10.3390/membranes2010040>
- McArthur SL, McLean KM, Kingshott P et al (2000) Effect of polysaccharide structure on protein adsorption. *Colloids Surf B Biointerfaces* 17:37–48. [https://doi.org/10.1016/S0927-7765\(99\)00086-7](https://doi.org/10.1016/S0927-7765(99)00086-7)
- Monchaux E, Vermette P (2007) Development of dextran-derivative arrays to identify physico-chemical properties involved in biofouling from serum. *Langmuir* 23:3290–3297. <https://doi.org/10.1021/la063012s>
- Müller MT, Yan X, Lee S et al (2005) Lubrication properties of a brushlike copolymer as a function of the amount of solvent absorbed within the brush. *Macromolecules* 38:5706–5713. <https://doi.org/10.1021/ma0501545>
- Nalam PC, Daikhin L, Espinosa-Marzal RM et al (2013) Two-fluid model for the interpretation of quartz crystal microbalance response: tuning properties of polymer brushes with solvent mixtures. *J Phys Chem C* 117:4533–4543. <https://doi.org/10.1021/jp310811a>

- Orgovan N, Patko D, Hos C et al (2014) Sample handling in surface sensitive chemical and biological sensing: a practical review of basic fluidics and analyte transport. *Adv Colloid Interface Sci* 211:1–16. <https://doi.org/10.1016/j.cis.2014.03.011>
- Peppas NA, Van Blarcom DS (2016) Hydrogel-based biosensors and sensing devices for drug delivery. *J Control Release* 240:142–150. <https://doi.org/10.1016/j.jconrel.2015.11.022>
- Perrino C (2009) Poly(L-lysine)-g-dextran (PLL-g-dex): brush-forming, biomimetic carbohydrate chains that inhibit fouling and promote lubricity
- Piehler J, Brecht A, Hehl K, Gauglitz G (1999) Protein interactions in covalently attached dextran layers. *Colloids Surf B Biointerfaces* 13:325–336. [https://doi.org/10.1016/S0927-7765\(99\)00046-6](https://doi.org/10.1016/S0927-7765(99)00046-6)
- Rivière JC, Myhra S (eds) (1998) *Handbook of surface and interface analysis*, 1st edn. Marcel Dekker, New York
- Saftics A (2018) Development of dextran-based hydrogel layers for biosensor applications. Budapest University of Technology and Economics
- Saftics A, Kurunczi S, Szekevényes Z et al (2016) Fabrication and characterization of ultrathin dextran layers: Time dependent nanostructure in aqueous environments revealed by OWLS. *Colloids Surf B Biointerfaces* 146:861–870. <https://doi.org/10.1016/j.colsurfb.2016.06.057>
- Saftics A, Kurunczi S, Türk B et al (2017) Spin coated carboxymethyl dextran layers on TiO₂-SiO₂ optical waveguide surfaces. *Rev Roum Chim* 62:775–781
- Saftics A, Prósz GA, Türk B et al (2018) In situ viscoelastic properties and chain conformations of heavily hydrated carboxymethyl dextran layers: a comparative study using OWLS and QCM-I chips coated with waveguide material. *Sci Rep* 8:11840. <https://doi.org/10.1038/s41598-018-30201-6>
- Saftics A, Türk B, Sulyok A et al (2019) Biomimetic dextran-based hydrogel layers for cell micropatterning over large areas Using the FluidFM BOT technology. *Langmuir* 35:2412–2421. <https://doi.org/10.1021/acs.langmuir.8b03249>
- Sauerbrey G (1959) Verwendung von Schwingquarzen zur Wagungdiinner Schichten und zur Mikrowagung. *Zeitschrift fur Phys* 155:206–222. <https://doi.org/10.1007/BF01337937>
- Secret E, Kelly SJ, Crannell KE, Andrew JS (2014) Enzyme-responsive hydrogel microparticles for pulmonary drug delivery. *ACS Appl Mater Interfaces* 6:10313–10321. <https://doi.org/10.1021/am501754s>
- Sidobre S, Puzo G, Rivière M (2002) Lipid-restricted recognition of mycobacterial lipoglycans by human pulmonary surfactant protein A: a surface-plasmon-resonance study. *Biochem J* 365:89–97. <https://doi.org/10.1042/bj20011659>
- Sivakumaran D, Maitland D, Hoare T (2011) Injectable microgel-hydrogel composites for prolonged small-molecule drug delivery. *Biomacromolecules* 12:4112–4120. <https://doi.org/10.1021/bm201170h>
- Stengel G, Höök F, Knoll W (2005) Viscoelastic modeling of template-directed DNA synthesis. *Anal Chem* 77:3709–3714. <https://doi.org/10.1021/ac048302x>
- Tanaka M, Hayashi T, Morita S (2013) The roles of water molecules at the biointerface of medical polymers. *Polym J* 45:701–710. <https://doi.org/10.1038/pj.2012.229>
- Tavakoli J, Tang Y (2017) Hydrogel based sensors for biomedical applications: an updated review. *Polymers (Basel)* 9:364. <https://doi.org/10.3390/polym9080364>
- Vogt BD, Lin EK, Wu WI, White CC (2004) Effect of film thickness on the validity of the sauerbrey equation for hydrated polyelectrolyte films. *J Phys Chem B* 108:12685–12690. <https://doi.org/10.1021/jp0481005>
- Voinova MV, Rodahl M, Jonson M, Kasemo B (1999) Viscoelastic acoustic response of layered polymer films at fluid-solid interfaces: continuum mechanics approach. *Phys Scr* 59:391–396. <https://doi.org/10.1238/Physica.Regular.059a00391>
- Vörös J (2004) the density and refractive index of adsorbing protein layers. *Biophys J* 87:553–561. <https://doi.org/10.1529/biophysj.103.030072>
- Xu C, Lee W, Dai G, Hong Y (2018) Highly elastic biodegradable single-network hydrogel for cell printing. *ACS Appl Mater Interfaces* acsami.8b01294. <https://doi.org/10.1021/acsami.8b01294>

- Zhang J, Horváth C (2003) Capillary electrophoresis of proteins in dextran-coated columns. *Electrophoresis* 24:115–120. <https://doi.org/10.1002/elps.200390002>
- Zhang YS, Khademhosseini A (2017) Advances in engineering hydrogels. *Science* (80–): 356:eaaf3627. <https://doi.org/10.1126/science.aaf3627>
- Zhang R, Tang M, Bowyer A et al (2005) A novel pH- and ionic-strength-sensitive carboxy methyl dextran hydrogel. *Biomaterials* 26:4677–4683. <https://doi.org/10.1016/j.biomaterials.2004.11.048>